

Direct Visualization of Laser-Driven Focusing Shock Waves

T. Pezeril,^{1,3,*} G. Saini,² D. Veysset,^{1,3} S. Kooi,³ P. Fidkowski,⁴ R. Radovitzky,⁴ and Keith A. Nelson³

¹*Laboratoire de Physique de l'Etat Condensé, UMR CNRS 6087, Université du Maine, 72085 Le Mans, France*

²*Department of Materials Science and Engineering, Massachusetts Institute of Technology, Cambridge, Massachusetts 02139, USA*

³*Department of Chemistry, Massachusetts Institute of Technology, Cambridge, Massachusetts 02139, USA*

⁴*Department of Aeronautics and Astronautics, Massachusetts Institute of Technology, Cambridge, Massachusetts 02139, USA*

(Received 22 March 2011; published 24 May 2011)

Direct real-time visualization and measurement of laser-driven shock generation, propagation, and 2D focusing in a sample are demonstrated. A substantial increase of the pressure at the convergence of the cylindrical acoustic shock front is observed experimentally and simulated numerically. Single-shot acquisitions using a streak camera reveal that at the convergence of the shock wave in water the supersonic speed reaches Mach 6, corresponding to the multiple gigapascal pressure range ~ 30 GPa.

DOI: 10.1103/PhysRevLett.106.214503

PACS numbers: 47.40.Nm, 43.25.Yw, 62.50.Ef

Cylindrically or spherically focusing shock waves have been of keen interest for the past several decades. In addition to the fundamental study of materials under extreme conditions [1–10], cavitation, and sonoluminescence [11,12], focusing shock waves enable a myriad of applications including hypervelocity launchers, synthesis of new materials, production of high-temperature and high-density plasma fields [13], applications in controlled thermonuclear fusion [14], and a variety of medical therapies [15]. The use of pulsed lasers to excite shock waves has considerably widened the possibilities for study of shock propagation and the dynamic properties of materials under shock loading [16]. In almost all laser shock research conducted to date, an intense light pulse irradiates a thin layer of material (such as aluminum) which, through ablation or chemical decomposition, acts as a shock transducer and launches a shock pulse into an underlying material layer or substrate that includes the sample of interest [17]. The shocked sample is typically probed optically from the opposite side through interferometric and/or spectroscopic measurements [18]. However, the different sample regions at which the shock wave arrives at different times are not resolved spatially in the measurement. Spatially distinct probing regions will enable shock imaging [19] as well as wide-ranging spectroscopic measurements spanning many spectral regions. Here we demonstrate laser-induced 2D focusing shock waves and direct, real-time visualization of shock-wave generation, in-plane propagation and focusing, and induced material responses [20]. Following pulsed laser excitation of a thin sample, the shock wave propagates laterally in the plane of the sample rather than through the sample plane as in the front-back approach described above. In the present case, the optical excitation or laser “shock” pulse is focused to a circular ring pattern at the sample, launching a shock wave that propagates and focuses inward toward the center. We present results from water solutions in which shock speeds reach Mach 6, corresponding to about 30 GPa at the vicinity of the shock focus.

The experimental setup and typical 2D images are shown in Fig. 1. A 300 ps, 800 nm laser shock pulse was directed onto an axicon conical prism (Doric Lenses Inc.) and focused by a lens with a 3 cm focal length to form a ring pattern at the sample layer. The ring had a 200 μm diameter, and the beam at any part of the ring had a width of ~ 10 μm . 2D spatial images of the propagating shock waves were recorded with a variably delayed 180 fs, 400 nm probe pulse that was directed through the sample and a conventional two-lens imaging system to a CCD camera. For interferometric imaging as shown in Fig. 1(a), the imaging probe was recombined interferometrically with the reference probe before reaching the camera. In some measurements, a streak camera (Hamamatsu C5680-21) and a 200 ns, 532 nm probe pulse derived from the laser that pumps the Ti:sapphire amplifier, were used for continuous-time imaging of a linear segment of the shock-wave trajectory extending from opposite sides of the irradiated ring to the focus. In the present experiments, the sample consisted of a 5 μm thick water layer with absorbing suspended carbon nanoparticles made from ink (China Black Ink, Majuscule) [21] diluted 10x so that the nanoparticle loading was about 2 wt% that was sandwiched between two 100 μm glass substrates using a polymer spacer. The shock wave is generated directly within the sample layer through absorption of the picosecond laser shock pulse by carbon nanoparticles that undergo photoreactive energy release and vaporization to generate high pressure [21–24]. We measured that 90% of the incident fluence was absorbed by the 5 μm thick sample layer. The impedance mismatch between the windows and the water sample confines a shock wave laterally in the sample plane.

CCD camera images of sample regions irradiated by low excitation laser pulse energy (0.08 mJ) are shown in Fig. 1(b). The present imaging setup allows one exposure at a specified probe pulse time delay to be recorded each time the sample is irradiated and a shock wave is launched.

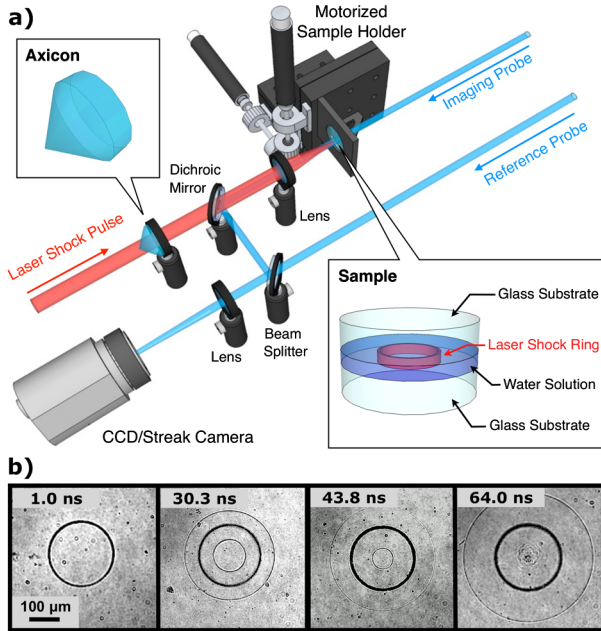


FIG. 1 (color online). (a) Schematic illustration of the experimental setup showing focusing shock-wave generation and imaging. The shock wave, generated directly in the sample layer, propagates laterally within the layer, and a Mach-Zehnder interferometer can be used as a probing tool to record images on the camera. The shock evolution is evaluated either from CCD or streak camera images. After each image is recorded, the target is shifted to a new position with a fresh area in the beam paths since each irradiated and shocked sample region is permanently damaged. (b) Raw CCD images recorded at various times after a water suspension of carbon nanoparticles was irradiated by an optical shock pulse of energy 0.08 mJ. The images clearly show shock responses propagating inward and outward from the irradiated region which appears as a dark ring due to bubble formation.

A time history is built up by single exposures taken at different sample positions with different time delays of the femtosecond probe pulse. Repeated measurements with the same time delay showed no significant variation. The recorded images can be used to extract the shock-wave propagation distance as a function of time, from which we can determine the shock speed U_s during the time interval between any two successive probe pulse delays or averaged over the entire traversal.

Interferometric images were recorded to quantitatively measure the inward and outward-propagating shock-wave positions and widths. Figure 2(a) shows images recorded at a fixed time delay of 25.3 ns following irradiation by excitation pulses with different energies. The inner wave clearly propagates faster toward the focus as the shock pulse energy is increased from 0.3 mJ to 2.0 mJ, reflecting the expected increase in speed as the shock pressure increases. The ring of bubbles around the excitation region also widens with increasing laser pulse energy. The results for shock-wave speed, averaged over 25.3 ns of traversal toward the focus, as a function of input laser pulse energy

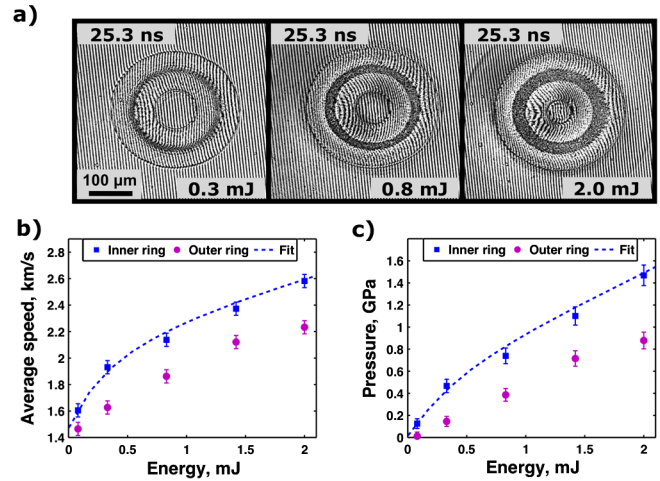


FIG. 2 (color online). (a) Interferometric images of liquid water at a fixed time delay of 25.3 ns with various optical shock pulse energies. The inner responses launched by higher-energy pulses have propagated farther toward the center of the ring because they have higher shock pressures and therefore higher speeds. (b) Plot of average speed and corresponding pressure (c) of the inner and outer shock waves as a function of shock pulse energy. The fitted values were calculated from finite element numerical simulations. The inner shock-wave propagates at a faster speed than the outer wave in all cases.

are depicted in Fig. 2(b). The inner wave propagated at a faster speed than the outer wave at all energy settings, and as is clear from Fig. 2(b) the propagation speed was higher at higher excitation pulse energies. The shock-wave peak pressure P in water is related to the propagation speed U_s through the equation of state and the jump conditions [25,26] at the shock front by

$$P = \rho_0 U_s \frac{U_s - c_0}{1.99} [\text{GPa}], \quad (1)$$

where $c_0 = 1.43$ km/s and $\rho_0 = 0.998$ g/cm³ denote the acoustic velocity and the density of the undisturbed water, respectively, the factor of 1.99 was determined empirically. Thus it is straightforward to calculate the pressure from the speed, yielding the results shown in Fig. 2(c). For the lowest laser pulse energy of 0.08 mJ, the outward-propagating wave was in the linear acoustic response limit with speed equal to c_0 . For the highest laser pulse energy, the shock wave propagated a distance toward the center of 65 μm in 25.3 ns, corresponding to a speed of almost Mach 2 at 2600 m/s and a pressure of 1.5 GPa.

The total time duration for shock propagation to the focus is many nanoseconds, making it impractical to record 2D CCD images (each from a distinct sample region) on a near-continuous basis. However, once it is established that the response is cylindrically symmetric as expected, a single spatial dimension is sufficient and the second dimension can be used for time in a streak camera recording that provides a continuous-time-resolved picture of the entire shock event as shown in Figs. 3(a)–3(c). In the streak images, not recorded interferometrically, the horizontal

dark lines at $\pm 100 \mu\text{m}$ are due to the bubbles at the excitation region, which gradually expand (with interface motion of about 500 m/s at the highest excitation pulse energy) during the observation period. At the shock front the refractive-index gradient is large and this leads to a deflection of the illuminating light from the imaging aperture, resulting in the dark appearance of the shock waves. The outer shock waves appear as dark lines that rapidly leave the field of view. The inner waves of primary interest appear as dark crossing lines with gradually increasing slopes. The shock position as a function of time was extracted from the streak images by an automated

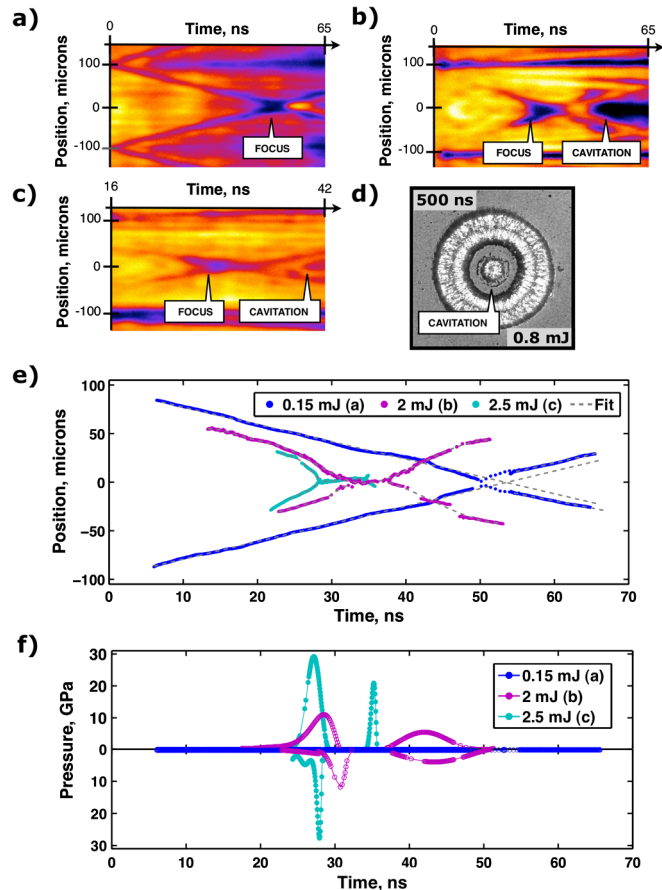


FIG. 3 (color online). Single-shot streak images of cylindrically focusing shock waves propagating in water at shock laser pulse energies of (a) 0.15, (b) 2.0, and (c) 2.5 mJ. (d) Snapshot image of the shocked sample at 500 ns time delay for a laser shock pulse energy of 0.8 mJ. Cavitation is responsible for bubble formation at the focus. (e) Trajectories of the converging shock waves extracted from streak images a) b) and c) by a best-fit polynomial equation. The radial distance on the vertical axis is measured from the center of convergence. (f) Pressure values calculated from fits of the trajectories in (e) using Eq. (1). The traces above and below the zero-pressure horizontal line represent the pressure values for the upper and lower trajectories shown in (e), derived from the upper and lower streak camera images of shock propagation from opposite sides of the excitation ring toward the center. The y-axis pressure values that appear above and below the zero-pressure line are all positive.

extraction routine. The resulting curves were then least squares fitted to polynomial functions which were differentiated with respect to time to yield shock-wave velocities that were then converted to shock pressures with the aid of Eq. (1). Figure 3(e) shows the corresponding raw trajectories and fitted polynomial trajectories extracted through image analysis. There is a jog in the 0.15 mJ trajectory as the shock wave moves through the focus, apparent in Fig. 3(a) and highlighted by the dotted lines in Fig. 3(e), that we believe is due to the Gouy phase shift, a well-known occurrence that has been observed through imaging of converging terahertz waves [27] and surface acoustic waves [28–30]. The two higher-power trajectories in Figs. 3(b) and 3(c) clearly reveal the acceleration and deceleration of the shock front as it reaches the center of convergence. In each of these cases there is a pronounced jog at the focus that lasts for several nanoseconds. This is likely due to cavitation as the shock front at the focus is followed by tensile strain that could bring the pressure below the vapor pressure for water and trigger bubble formation [11]. As shown in Fig. 3(d), CCD images recorded at long delay times (even at the lowest laser shock pulse energy) clearly show a bubble at the focus as well as an expanded bubble around the irradiated region.

At 2.5 mJ excitation pulse energy, the shock speed rapidly increases and reaches about 9 km/s, or Mach 6, near the focus at 28 ns. Through Eq. (1), the corresponding pressure is ~ 30 GPa as shown in Fig. 3(f). The corresponding temperature is ~ 2500 K based on the known properties of water under shock loading, described by $P - T$ Hugoniot curve [16,26]. The pressure reached exactly at the focus is expected to be even higher, but as in single-bubble sonoluminescence experiments [12] the peak pressure cannot be determined accurately. To overcome this limitation and to gain a greater understanding of shock-wave propagation in the experiments, we performed finite element numerical simulations. We used the Tait equation of state [31,32] for a Newtonian fluid to model the water, with viscosity introduced phenomenologically to suppress shock singularity. The continuum equations were integrated by an explicit Newmark method [33], and an updated Lagrangian scheme was employed to establish the initial pressure as an eigenstrain. The water $P - \rho$ Hugoniot curve was used to calculate the peak pressure at any point during the trajectory from the simulated peak density. To correlate the initial pressures to the laser shock pulse energies used in the experiments, we assumed a linear relationship and matched computed and experimental trajectories to calculate the proportionality constant. Simulations with various initial pressures yielded the dashed curves in Figs. 2(b) and 2(c). Figure 4 shows the results of one simulation in more detail. The pressures reached by the inner and outer shock waves as they propagated away from the initial ring are shown, along with the shock-wave profiles (inset) at various times during propagation. The simulated wave profiles shown in Figure 4(a) (inset) indicate that the shock wave builds up almost

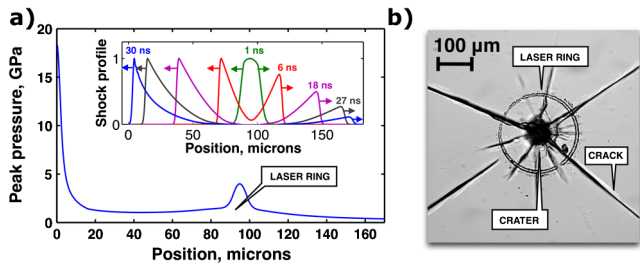


FIG. 4 (color online). (a) Numerical simulation of shock-wave peak pressure and (inset) normalized pressure profiles at different times in water as a function of radial distance from the shock focus at $0 \mu\text{m}$. The simulation was based on a laser pulse energy of 2 mJ . (b) Typical optical microscope image of sample damage around the focus for a shock pulse energy of 1.5 mJ or higher (2 mJ was used for this image). The crater at the shock focus goes through the entire $100 \mu\text{m}$ thick glass substrate. The cracks extend outward up to 5 mm .

immediately and displays a characteristic sharp rising front of $4 \mu\text{m}$ spatial extent which remains constant until reaching the center where it sharpens down to $3 \mu\text{m}$. These values may be limited in part by convolution with the grid size of $1 \mu\text{m}$. In contrast, the outer shock front broadens up to $6 \mu\text{m}$, showing that the geometrical acoustic diminishment substantially moderates shock propagation. At the center of convergence, the pressure increases sharply up to 18 GPa —more than a factor of 4 higher than the initial pressure at the irradiated region and more than a factor of 10 greater than the pressure just outside the central region—due to the 2D focusing. Although we do not have a reliable experimental measurement of the pressure at the focus, there are clear indications of sharply increased pressure there including severe sample damage as shown in Fig. 4(b). We note that no light emission at the shock focus was observed even when we used laser irradiation to create a bubble at the center of convergence prior to launching the shock wave. This is consistent with evidence indicating that sonoluminescence results from bubble dynamics and collapse in restricted ranges of pressure and other parameters that are typically distinct from shock compression [12].

Spatially resolved images of laterally propagating laser-induced shock waves and single-shot streak camera measurements of shock-wave trajectories have been recorded. Results in water solution and numerical simulations indicate shock speeds up to Mach 6 and shock pressures up to several tens of GPa near the focus of a converging 2D shock wave launched with a laser pulse energy of several mJ. In the present experiments, shock propagation has been characterized. Spatially and temporally resolved spectroscopic measurements of materials under shock loading, using light in nearly any spectral region including THz, IR, visible, or UV, are now possible, with the shock pressure, duration, and profile under experimental control through the pump laser intensity, linewidth,

and profile. Measurements of solid samples, on a single substrate or freestanding, and measurements of chemical and structural transformations at the shock focus will be reported subsequently.

This work was supported by the U.S. Army through the Institute for Soldier Nanotechnologies, under Contract DAAD-19-02-D-0002. We thank A. Lomonosov, A. Maznev, and V. Tournat for fruitful comments and suggestions.

*thomas.pezeril@univ-lemans.fr

- [1] K. G. Guderley, *Luftfahrtforschung* **19**, 302 (1942).
- [2] R. W. Perry and A. Kantrowitz, *J. Appl. Phys.* **22**, 878 (1951).
- [3] K. P. Stanyukovich, *Unsteady Motion of Continuous Media* (Pergamon Press, Oxford, 1960).
- [4] J. H. Lee and B. H. K. Lee, *Phys. Fluids* **8**, 2148 (1965).
- [5] H. Matsuo, *Phys. Fluids* **22**, 1618 (1979).
- [6] M. Van Dyke and A. J. Guttman, *J. Fluid Mech.* **120**, 451 (1982).
- [7] K. Takayama *et al.*, *Exp. Fluids* **5**, 315 (1987).
- [8] M. Watanabe and K. Takayama, *Shock Waves* **1**, 149 (1991).
- [9] V. Eliasson *et al.*, *Shock Waves* **15**, 205 (2006).
- [10] A. Ramu, M. P. Ranga Rao, *J. Eng. Math.* **27**, 411 (1993).
- [11] R. Pecha and B. Gompf, *Phys. Rev. Lett.* **84**, 1328 (2000).
- [12] M. Brenner *et al.*, *Rev. Mod. Phys.* **74**, 425 (2002).
- [13] H. Matsuo and Y. Nakamura, *J. Appl. Phys.* **51**, 3126 (1980); *J. Appl. Phys.* **52**, 4503 (1981).
- [14] M. Schirber, *Science* **310**, 1610 (2005).
- [15] K. Takayama and T. Saito, *Annu. Rev. Fluid Mech.* **36**, 347 (2004).
- [16] M. Koenig *et al.*, *Nucl. Fusion* **44**, S208 (2004).
- [17] D. D. Dlott, *Annu. Rev. Phys. Chem.* **50**, 251 (1999).
- [18] K. T. Gahagan *et al.*, *J. Appl. Phys.* **92**, 3679 (2002).
- [19] A. V. Lukashev *et al.*, *Proc. SPIE Int. Soc. Opt. Eng.* **1121**, 201 (1989).
- [20] G. Saini, Ph.D. Dissertation, MIT (2010).
- [21] A. M. Lomonosov, V. Mikhalevich, P. Hess, and E. Knight, *J. Acoust. Soc. Am.* **105**, 2093 (1999).
- [22] Y. Yang *et al.*, *Appl. Phys. Lett.* **85**, 1493 (2004).
- [23] J. E. Patterson *et al.*, *Shock Waves* **14**, 391 (2005).
- [24] C. Frez and G. J. Diebold, *J. Chem. Phys.* **129**, 184506 (2008).
- [25] S. Katsuki *et al.*, *Jpn. J. Appl. Phys.* **45**, 239 (2006).
- [26] K. Nagayama *et al.*, *J. Appl. Phys.* **91**, 476 (2002).
- [27] T. Feurer *et al.*, *Phys. Rev. Lett.* **88**, 257402 (2002).
- [28] C. K. Jen *et al.*, *Appl. Phys. Lett.* **46**, 241 (1985).
- [29] N. C. R. Holme *et al.*, *Appl. Phys. Lett.* **83**, 392 (2003).
- [30] C. Glorieux *et al.*, *Rev. Sci. Instrum.* **75**, 2906 (2004).
- [31] V. K. Kedrinskii, *Hydrodynamics of Explosion* (Springer-Verlag, Berlin, Germany, 2005).
- [32] W. C. Davis, *Shock Waves; Rarefaction Waves; Equations of State* (Springer-Verlag, New York, 1997).
- [33] *Computational Methods for Transient Analysis*, edited by T. Belytschko and T. J. R. Hughes (North-Holland, Amsterdam, 1983).